Radiation Dosimetry and Biodistribution of ^{18}F-PSMA-11 for PET Imaging of Prostate Cancer

Sarah Piron[1], Kathia De Man[2], Nick Van Laeken[2], Yves D'Asseler[2], Klaus Bacher[3], Ken Kersemans[2], Piet Ost[4], Karel Decaestecker[5], Pieter Deseyne[4], Valérie Fonteyne[4], Nicolaas Lumen[5], Eric Achten[2], Boudewijn Brans[2], and Filip De Vos[1]

[1]Laboratory of Radiopharmacy, Ghent University, Ghent, Belgium; [2]Department of Nuclear Medicine, Ghent University Hospital, Ghent, Belgium; [3]Department of Human Structure and Repair, Ghent University Hospital, Ghent, Belgium; [4]Department of Radiation Oncology, Ghent University Hospital, Ghent, Belgium; and [5]Department of Urology, Ghent University Hospital, Ghent, Belgium

Prostate-specific membrane antigen (PSMA) is highly overexpressed in prostate cancer. Many PSMA analog radiotracers for PET/CT prostate cancer staging have been developed, such as ^{68}Ga-PSMA-11. This radiotracer has achieved good results in multiple clinical trials, but because of the superior imaging characteristics of ^{18}F-fluoride, ^{18}F-PSMA-11 was developed. The aim of this study was to evaluate the administration safety and radiation dosimetry of ^{18}F-PSMA-11. **Methods:** Six patients (aged 62–68 y; mean, 66 ± 2 y) with suspected prostate cancer recurrence after previous treatment were administered 2 MBq of ^{18}F-PSMA-11 per kilogram of body weight and then underwent low-dose PET/CT imaging at 0, 20, 50, 90, and 300 min after injection. To evaluate the safety of administration, vital parameters were monitored. To assess toxicity, full blood count and biochemical parameters were determined. According to the latest International Commission on Radiological Protection recommendations, radiation dosimetry analysis was performed using IDAC-Dose 2.1. For blood activity measurement, small samples of venous blood were collected at various time points after injection. The unbound ^{18}F-fluoride fraction was determined in plasma at 20, 50, and 90 min after administration to evaluate the defluorination rate of ^{18}F-PSMA-11. **Results:** After injection, ^{18}F-PSMA-11 cleared rapidly from the blood. At 5 h after injection, 29.0% ± 5.9% of the activity was excreted in urine. The free ^{18}F fraction in plasma increased from 9.7% ± 1.0% 20 min after injection to 22.2% ± 1.5% 90 min after injection. The highest tracer uptake was observed in kidneys, bladder, spleen, and liver. No study drug–related adverse events were observed. The calculated mean effective dose was 12.8 ± 0.6 μSv/MBq. **Conclusion:** ^{18}F-PSMA-11 can be safely administered and results in a mean effective dose of 12.8 ± 0.6 μSv/MBq. Therefore, the total radiation dose is lower than for other PSMA PET agents and in the same range as ^{18}F-DCFPyL.

Key Words: dosimetry; PSMA; ^{18}F-PSMA-11; PET/CT; prostate cancer

J Nucl Med 2019; 60:1736–1742
DOI: 10.2967/jnumed.118.225250

In men, prostate cancer is the second most frequently diagnosed cancer worldwide (*1*). A major issue in clinical management is early detection of recurrent disease after radical prostatectomy or local therapy with curative intent. Approximately 30% of patients undergoing radical prostatectomy experience biochemical recurrence within 10 y (*2*). Usually, this recurrence first presents itself through an increased serum prostate-specific antigen level (*3*). However, for salvage therapy to be successful, precise localization of metastases is necessary to determine the most appropriate treatment. Because prostate-specific antigen levels make no distinction between local and systemic disease, there is a need for reliable imaging biomarkers to determine the exact location of metastatic tumors (*4,5*).

Limitations of currently used imaging probes have led to a growing interest in new PET tracers for improved imaging of prostate cancer metastases (*6,7*). Over the last few years, prostate-specific membrane antigen (PSMA) has gained a lot of interest as a specific target for prostate cancer imaging. Although PSMA is also expressed in normal prostate tissue and in other organs such as the small intestine, salivary glands, and kidneys, the expression level in both primary and metastatic prostate cancer is 100- to 1,000-fold higher (*8–10*).

Good results have been achieved with the recently developed radiotracer Glu-NH-CO-NH-Lys-(Ahx)-^{68}Ga-(HBED-CC) (^{68}Ga-PSMA-11) which is recommended for restaging of biochemically recurrent prostate cancer (*11–13*). However, whereas ^{68}Ga as a PET isotope is beneficial for centers without a cyclotron, its use is associated with several disadvantages such as the short lifespan of the ^{68}Ge/^{68}Ga generator, the limited patient doses per generator elution, and the short half-life. Additionally, the high positron energy of ^{68}Ga (E_{max}, 1.899 MeV) contributes to the larger positron range, which decreases the spatial resolution of the PET images, whereas the low positron yield (87.7%) leads to a reduced sensitivity. These limitations make detection of small metastatic lesions with low PSMA expression difficult (*14–16*).

Therefore, there is an increased demand for the development and clinical validation of ^{18}F-labeled PSMA-targeting radiotracers such as ^{18}F-DCFBC (*17*), ^{18}F-DCFPyl (*18*), and ^{18}F-PSMA-1007 (*19*). However, these radiotracers encounter disadvantages such as high blood-pool activity, regional patent protection, and slow excretion kinetics, respectively. To overcome these issues, ^{18}F-PSMA-11 was introduced by Malik et al. (*20*) and Boschi et al. (*21*). The precursor (PSMA-11) is readily available, and a good-manufacturing-practice–compliant radiosynthesis was recently developed by Kersemans

Received Jan. 2, 2019; revision accepted Apr. 25, 2019.
For correspondence or reprints contact: Sarah Piron, Ghent University, Ottergemsesteenweg 460, 9000 Ghent, BE-Belgium.
E-mail: sarah.piron@ugent.be
Published online Apr. 26, 2019.

TABLE 1
Patient Characteristics

Patient no.	Age (y)	Weight (kg)	PSA (ng/mL)	Gleason score	Medical history
1	67	56	0.3	7 (4 + 3)	Radical prostatectomy
2	67	114	1.1	5 (2 + 3)	Primary radiotherapy
3	68	90	42.5	7 (3 + 4)	Radical prostatectomy + postoperative radiotherapy and salvage lymph node dissection
4	66	99	19.0	9 (4 + 5)	Pelvic lymph node dissection + primary radiotherapy + androgen deprivation therapy; castration-resistant prostate cancer with rising PSA under abiraterone, 1,000 mg/d, and prednisone, 5 mg twice per day
5	66	81	5.0	7 (4 + 3)	Radical prostatectomy, adjuvant radiotherapy at prostate bed
6	62	80	0.5	9 (4 + 5)	Radical prostatectomy, radiotherapy, androgen deprivation therapy

PSA = prostate-specific antigen level.

et al. (*14*), which allows for large-scale production and implementation in clinical routine. Although the synthesis of this compound has been thoroughly investigated (*14,20–22*), no clinical data on first human administration have yet been published.

The aim of this study was to assess the administration safety and biodistribution of ^{18}F-PSMA-11 in humans. Secondary goals were to determine the radiotracer kinetics and metabolites in plasma and urine, establish critical organs, and calculate the organ dosimetry and total-body effective dose.

MATERIALS AND METHODS

The study was approved by the Ethics Committee of the Ghent University Hospital (2017/1294) and conducted following the International Conference on Harmonisation Good Clinical Practice E6 (R2) guidelines and the Declaration of Helsinki (EudraCT number 2017-003461-96). The study was supported by the Flemish foundation FWO TBM (T001517). All subjects gave written consent before participating in the study.

Six patients (aged 62–68 y; median, 66.5 y) with biochemical recurrence after curative treatment (prostatectomy with or without lymphadenectomy or radiotherapy) were prospectively enrolled in the study during a consultation with their treating physician. Patients who were under 40 or above 70 y old, were physically or mentally unfit to perform the planned procedures, or refused to be informed about accidental findings on scans were excluded from the study. Patient characteristics are provided in Table 1.

To evaluate the safety of ^{18}F-PSMA-11 administration, vital parameters such as body temperature, blood pressure, and heart rate were measured at multiple time points up to 5 h after injection. To determine toxicity, a full blood count was performed, as well as measurement of sodium, creatinine, alanine aminotransferase, and alkaline phosphatase before and 300 min after administration of ^{18}F-PSMA-11. Adverse events were reported up to 24 h after injection according to the Common Terminology Criteria for Adverse Events (CTCAE) scoring system, version 4.0.

PET/CT imaging was performed using a GE Healthcare Discovery MI 3-ring system, which is a digital PET/CT scanner with silicon photomultiplier–based PET detectors coupled to lutetium-based scintillators, an axial field of view of 15 cm, and a measured resolution of around 4.5 mm. ^{18}F-PSMA-11 was synthesized as described by Kersemans et al. (*14*). After intravenous injection of 2.0 ± 0.2 MBq of ^{18}F-PSMA-11 per kilogram of body weight, a whole-body PET scan was acquired, followed by additional imaging at 20, 50, 90, and 300 min after radiotracer injection. PET emission times varied from 45 s (scan at time of injection and 20 min after injection) to 80 s (scan at 50 min after injection) and 2 min (scan at 90 and 300 min after injection) per bed position. Each PET scan was preceded by a low-dose CT scan (100 keV, 30 mAs) for attenuation correction. The PET scans were reconstructed using QClear (GE Healthcare), which is a block sequential regularized expectation maximization algorithm (*23*). The reconstruction takes into account time-of-flight information, point-spread function compensation, and CT-based attenuation and scatter correction; a β-parameter of 600 was chosen.

To determine the clearance rate from the blood, small venous blood samples (collected at 5, 10, 20, 30, 50, 70, 90, and 300 min after injection) were measured using a calibrated γ-counter (Cobra; Packard). Additionally, patients were asked to empty the bladder before administration of the radiotracer, followed by collection of the excreted urine at 90, 180, and 300 min after injection. At each time point, a sample was measured using a calibrated γ-counter (Cobra).

Defluorination of ^{18}F-PSMA-11 was determined by collection of an additional blood sample at 20, 50, and 90 min after injection. Blood samples were centrifuged at 4,000 rpm for 10 min at 4°C. After collection of the supernatant, 1 mL of plasma was diluted 1:5 with 0.05 M acetate buffer, pH 4.5, and loaded onto 2 Oasis HLB columns

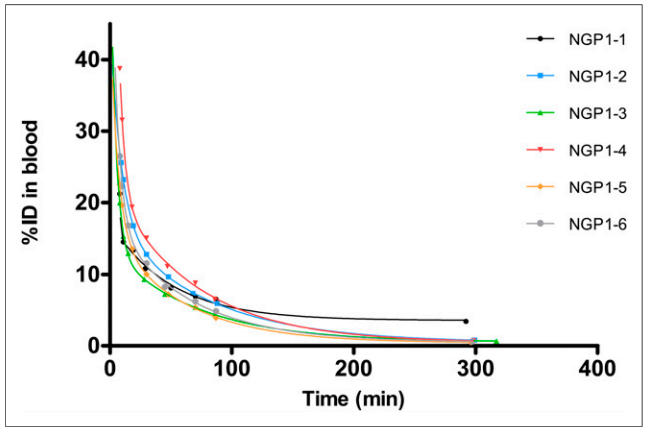

FIGURE 1. Time–activity curves in whole blood. NGP = patient.

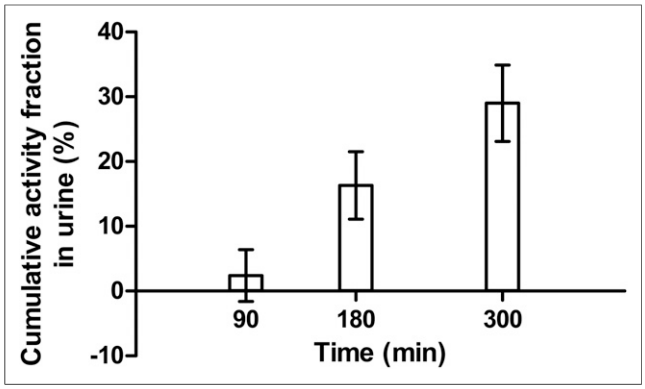

FIGURE 2. Mean cumulative activity in urine.

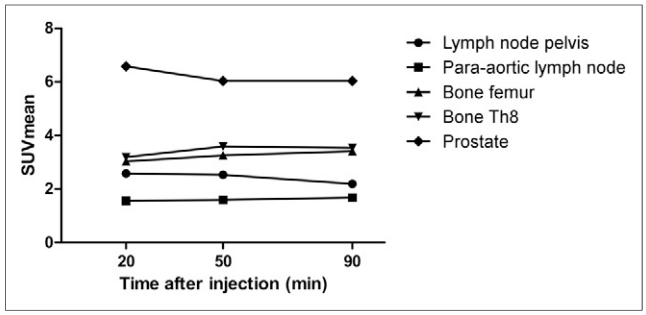

FIGURE 4. SUV_{mean} over time for 5 suspected lesions.

(Waters) in tandem, which were preconditioned with 10 mL of 70% ethanol and 10 mL of Milli-Q H_2O (Millipore). Finally, the columns were washed with 2 × 4 mL Milli-Q H_2O. The spillover and wash were collected, and activity was measured using a calibrated γ-counter (Cobra), as these fractions represent the free fraction of ^{18}F-fluoride. The results were expressed as percentage free ^{18}F-fluoride.

On the basis of the fused PET/CT data, we manually delineated volumes of interest for bone, liver, kidneys, spleen, lacrimal glands, parotis glands, submandibular glands, aortic arch, pancreas, lungs, brain, and total body using the Mirada Simplicit^{90}Y software (build 1.1.0.26641; Mirada Medical). To examine the biodistribution of the radiotracer, time–activity curves were calculated by determining the radioactivity concentration for each organ, correcting it for decay, and plotting it versus time. Subsequently, a time-integrated activity coefficient was determined for each organ by fitting the time–activity curves with a single-exponential or biexponential function using SPSS, version 25 (IBM). Internal organ doses were calculated with IDAC-Dose 2.1 software, which estimates the organ dose based on earlier published photon-specific absorbed fractions for the International Commission on Radiological Protection male adult reference computational voxel phantom (*24*). For determining the absorbed dose of the bladder, a voiding interval of 3 h was used. Finally, the effective dose was calculated using International Commission on Radiological Protection Publication 103 tissue weighting factors (*25*).

RESULTS

The radiochemical purity of the final formulation was determined using thin-layer chromatography and high-performance liquid chromatography and exceeded 95% and 98%, respectively. The mean administered mass of PSMA-11 was 2.9 ± 1.2 μg. The mean injected activity of ^{18}F-PSMA-11 was 1.91 ± 0.10 MBq/kg (mean total activity, 163.5 ± 33.5 MBq).

All 6 patients tolerated the drug product well. No clinically relevant changes in vital parameters were observed. Blood samples analyzed for hematology and biochemistry indicated no changes larger than the test method and within-subject biologic variability. The only exceptions were a high white blood cell count (grade 1 CTCAE) before administration of ^{18}F-PSMA-11 and an increase in serum creatinine levels (grade 1 CTCAE) at 5 h after ^{18}F-PSMA-11 administration in patient 3. None of the patients reported any side effects.

For each patient, the activity in whole blood was plotted as percentage injected dose (%ID) as a function of time (Fig. 1). The total blood volume was estimated using the reference book method (*26*), where 1 kg of body weight corresponds to 75 mL of blood. The radiotracer cleared rapidly from the blood. At 10 min after injection, 20.08 ± 5.2 %ID was still present in whole blood; this amount decreased to 10.89 ± 1.95 %ID after 30 min. The initial percentage of free ^{18}F-fluoride in plasma (4.2% ± 0.7%) increased to 9.7% ± 1.0%, 15.9% ± 2.0%, and 22.2% ± 1.5% at 20, 50, and 90 min after injection, respectively. The mean cumulative activity in urine was 2.4 ± 4.0 %ID, 16.3 ± 5.2 %ID, and 29.0 ± 5.9 %ID at 90, 180, and 300 min after injection, respectively (Fig. 2).

Immediately after administration of ^{18}F-PSMA-11, vascular structures and the kidneys could be observed (Fig. 3). Twenty minutes after injection, a physiologic high tracer uptake was detected in the lacrimal and salivary glands, kidneys, ureters, bladder, liver, and spleen. Physiologic moderate uptake was observed in the pancreas and intestines. In addition, all patients showed focal uptake in the skeleton (axial and peripheral), and 4 patients showed accumulation of activity in lymph node regions (paraaortic, parailiac, or inguinal). One patient showed uptake in the lungs, and 1 patient in the prostate region. The SUV_{mean} of focal uptake in 2 suggestive lymph nodes, 2 suggestive bone lesion, and suggestive prostate are presented in Figure 4. The highest SUV_{mean} at 50 min after injection was observed in the prostate (6.03), followed by both bone lesions (3.59 in T8 and 3.26 in the femur) and the lymph nodes (2.53 in pelvic and 1.59 in paraaortic). Figure 5 shows focal ^{18}F-PSMA uptake in the axial skeleton over time (20, 50, and 90 min after injection).

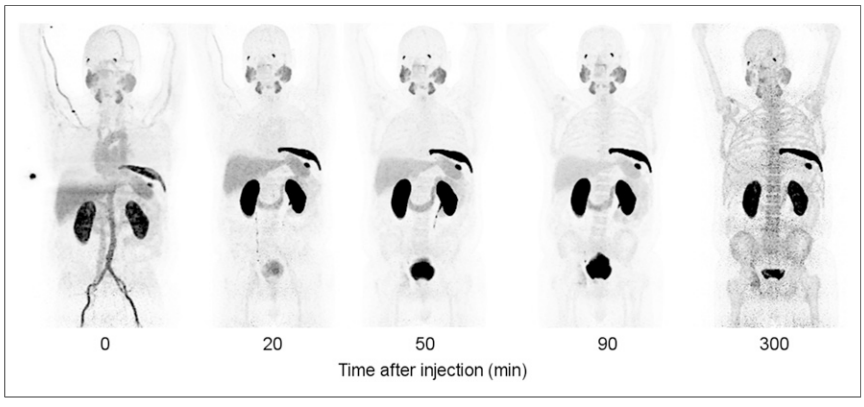

FIGURE 3. Overview of maximum-intensity-projection images at 0, 20, 50, 90, and 300 min after injection.

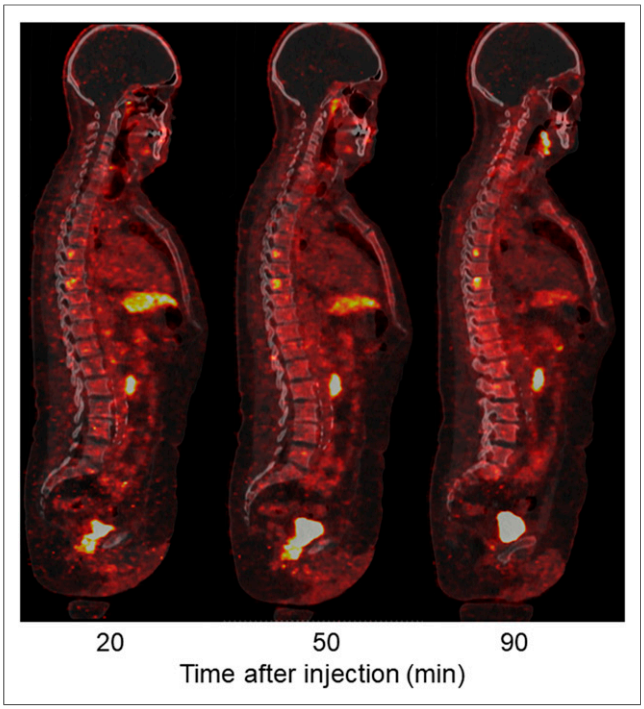

FIGURE 5. Low-dose PET/CT sagittal images of bone window. Two possible bone lesions can be detected at T6 and T8, as well as local recurrence in prostate bed.

Figure 6 demonstrates the biodistribution of ^{18}F-PSMA-11 in all major contributing organs, expressed as %ID per gram of tissue (%ID/g). The highest %ID/g was in the kidneys and bladder (maximum observed values, 0.0713 %ID/g and 0.0550 %ID/g, respectively). The %ID/g for all other organs did not exceed 0.015 %ID/g.

The mean total effective dose of ^{18}F-PSMA-11 was 12.8 ± 0.6 μSv/MBq, which results in an effective dose of 1.792 mSv for an average person of 70 kg who was administered a dose of 2 MBq/kg of body weight. Table 2 provides the estimated organ doses and effective doses for each patient. The highest mean tracer uptake was seen in the urinary bladder wall (0.126 ± 0.00327 mGy/MBq), the kidneys (0.0850 ± 0.0164 mGy/MBq), the prostate region (0.0470 ± 0.00124 mGy/MBq), and the salivary glands (0.0352 ± 0.0141 mGy/MBq). A comparison of the total effective dose and the absorbed dose per organ with other commonly used radiotracers is presented in Figures 7 and 8, respectively.

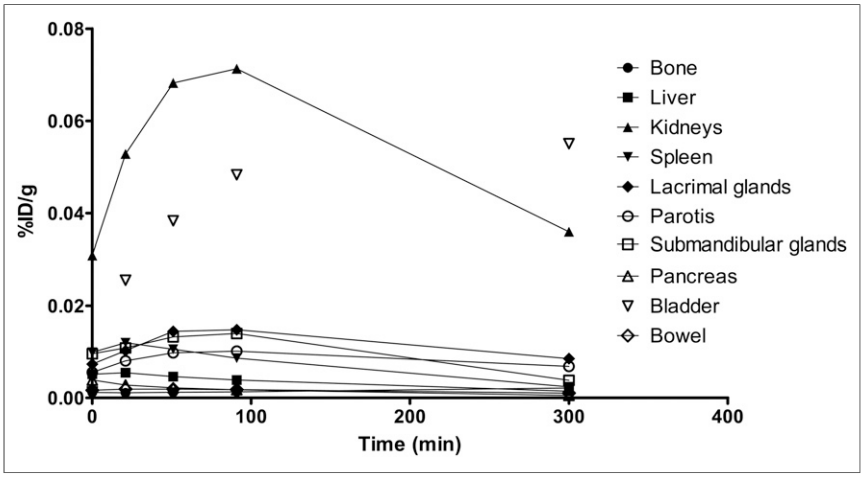

FIGURE 6. Time–activity curve of patient 5 for all major contributing organs.

DISCUSSION

Concerning the safety of administration of ^{18}F-PSMA-11, all patients tolerated the drug product well. The only exception was a grade 1 CTCAE increase in serum creatinine levels in patient 3. This increase is unlikely to be related to the study drug and can more likely be attributed to the consumption of a cooked meat meal by a diabetic patient between the 2 blood samples (before and after ^{18}F-PSMA-11 scanning) for serum creatinine determination. This type and degree of temporary deterioration of renal function after a cooked meal has been frequently described in the literature and was observed multiple times in this particular patient (*27,28*). The patient's kidney function was further monitored and recuperated well.

^{18}F-PSMA-11 demonstrates favorable radiotracer characteristics such as rapid clearance from the blood, which suggests fast distribution to tissues and elimination pathways. A high renal clearance rate could be seen after evaluation of urine samples, as 29.0% ± 5.9% of the injected activity was excreted 5 h after injection. This corresponds to the highest absorbed doses, which were measured in the urinary bladder wall (0.126 ± 0.00327 mGy/MBq) and the kidneys (0.0850 ± 0.0164 mGy/MBq). These absorbed doses are relatively low compared with other PSMA tracers, such as ^{68}Ga-PSMA-11 (0.130 and 0.262 mGy/MBq (*29*), respectively) and ^{18}F-PSMA-1007 (0.0187 and 0.170 mGy/MBq (*30*), respectively). ^{68}Ga-PSMA-11 shows a similar biodistribution to ^{18}F-PSMA-11 because of structural similarities. However, the lower positron energy of ^{18}F than of ^{68}Ga (0.65 vs. 1.90 MeV) gives a lower radiation dose (*15,29*). In a different dosimetry study, Pfob et al. (*31*) reported a similar absorbed dose between ^{68}Ga-PSMA-11 and ^{18}F-PSMA-11 (urinary bladder wall, 0.164 vs. 0.126 mGy/MBq; kidneys, 0.122 vs. 0.0850 mGy/MBq). However, these values are not directly comparable, as patients received 20 mg of furosemide to promote urinary excretion of the radiotracer. ^{18}F-PSMA-1007 is eliminated by hepatobiliary clearance, and one would expect low absorbed doses for kidney and bladder. However, the absorbed dose for kidney is twice as high for ^{18}F-PSMA-1007 as for ^{18}F-PSMA-11 because of retention of ^{18}F-PSMA-1007 in the kidney parenchyma (*30*). Comparison of the bladder absorbed dose between these 2 radiotracers is more difficult, as the time–activity curves for ^{18}F-PSMA-1007 were corrected for renal excretion of the activity (*30*). In dosimetry calculations, a voiding interval of 3 h was applied. Because prostate cancer patients are known for urinary incontinence, a urinary frequency of 8 times per day is an underestimation but ensures that the estimated radiation dose represents the worst-case scenario.

Figure 4 shows that the SUV_{mean} in the selected suspected lesions remained constant over time between 20 and 90 min after injection, suggesting retention of the radiotracer in these foci. However, as no diagnostic CT scan was performed, it is difficult to evaluate the nature of the focal-uptake lesions.

TABLE 2
Estimated Organ Doses and Effective Dose Using IDAC Dose 2.1

Organ	Patient 1-1	Patient 1-2	Patient 1-3	Patient 1-4	Patient 1-5	Patient 1-6	Mean	SD
Adrenals	1.39E−02	2.38E−02	1.81E−02	1.83E−02	1.97E−02	1.92E−02	1.88E−02	3.18E−03
Brain	1.71E−03	1.65E−03	1.35E−03	1.62E−03	1.69E−03	1.55E−03	1.60E−03	1.33E−04
Bronchi, total	2.29E−02	2.89E−02	2.29E−02	2.16E−02	2.05E−02	2.18E−02	2.31E−02	2.98E−03
Colon wall	9.58E−03	1.13E−02	9.47E−03	9.72E−03	1.00E−02	1.00E−02	1.00E−02	6.67E−04
Endosteum (bone surface)	4.94E−03	5.65E−03	4.34E−03	4.90E−03	4.70E−03	4.77E−03	4.88E−03	4.32E−04
Gallbladder wall	9.99E−03	1.47E−02	1.25E−02	1.01E−02	1.03E−02	1.11E−02	1.14E−02	1.85E−03
Heart wall	4.46E−03	6.19E−03	4.63E−03	4.24E−03	4.20E−03	4.39E−03	4.69E−03	7.54E−04
Kidneys	5.78E−02	1.06E−01	7.66E−02	8.69E−02	9.28E−02	8.97E−02	8.50E−02	1.64E−02
Left colon wall	4.26E−03	6.21E−03	4.52E−03	4.52E−03	4.80E−03	4.69E−03	4.83E−03	6.99E−04
Liver	1.45E−02	2.18E−02	2.01E−02	1.47E−02	1.48E−02	1.66E−02	1.71E−02	3.14E−03
Lung	9.81E−03	1.21E−02	9.88E−03	9.28E−03	8.75E−03	9.35E−03	9.86E−03	1.17E−03
Lymph nodes, total	2.70E−02	3.07E−02	2.42E−02	2.56E−02	2.53E−02	2.65E−02	2.66E−02	2.38E−03
Muscle	4.27E−03	5.08E−03	3.70E−03	4.06E−03	3.99E−03	4.05E−03	4.19E−03	4.72E−04
Pancreas	1.37E−02	1.19E−02	1.07E−02	9.20E−03	9.36E−03	9.91E−03	1.08E−02	1.74E−03
Prostate	4.76E−02	4.68E−02	4.48E−02	4.68E−02	4.81E−02	4.81E−02	4.70E−02	1.24E−03
Rectosigmoid colon wall	2.75E−02	2.74E−02	2.58E−02	2.70E−02	2.77E−02	2.77E−02	2.72E−02	7.25E−04
Red (active) bone marrow	7.79E−03	8.98E−03	7.38E−03	7.90E−03	7.80E−03	7.90E−03	7.96E−03	5.36E−04
Right colon wall	5.93E−03	8.24E−03	6.27E−03	6.27E−03	6.38E−03	6.51E−03	6.60E−03	8.26E−04
Salivary glands	5.09E−02	3.25E−02	1.69E−02	3.27E−02	2.56E−02	5.28E−02	3.52E−02	1.41E−02
Skin	2.39E−03	3.00E−03	1.96E−03	2.18E−03	2.11E−03	2.17E−03	2.30E−03	3.69E−04
Small intestine wall	1.15E−02	1.30E−02	1.12E−02	1.16E−02	1.20E−02	1.20E−02	1.19E−02	6.27E−04
Spleen	1.26E−02	2.76E−02	3.25E−02	1.50E−02	2.84E−02	2.01E−02	2.27E−02	8.01E−03
Stomach wall	5.00E−03	7.39E−03	5.92E−03	5.11E−03	5.47E−03	5.48E−03	5.73E−03	8.76E−04
Testes	4.48E−03	5.01E−03	3.65E−03	4.04E−03	4.02E−03	4.05E−03	4.21E−03	4.73E−04
Thymus	3.21E−03	4.09E−03	2.72E−03	2.94E−03	2.67E−03	2.86E−03	3.08E−03	5.30E−04
Thyroid	2.61E−03	3.24E−03	1.95E−03	2.29E−03	2.05E−03	2.26E−03	2.40E−03	4.70E−04
Urinary bladder wall	1.27E−01	1.23E−01	1.21E−01	1.25E−01	1.29E−01	1.29E−01	1.26E−01	3.27E−03
Remainder	5.52E−02	6.32E−02	4.82E−02	5.30E−02	5.04E−02	5.37E−02	5.40E−02	6.07E−03
Effective dose (mSv/MBq)	1.26E−02	1.41E−02	1.24E−02	1.24E−02	1.26E−02	1.28E−02	1.28E−02	6.46E−04

Data are mGy/MBq.

Measurement of the free ^{18}F-fluoride fraction in plasma indicated an increase of up to 22.2% ± 1.5% 90 min after injection. However, this elevated fraction of ^{18}F-fluoride is not reflected in a substantial increase in bone activity, as the mean percentage contribution of bone to whole-body activity increases by only 1.4% at 50 versus 20 min after injection and 2.5% at 90 versus 50 min after injection. This finding can be explained by rapid plasma clearance, renal excretion of ^{18}F-fluoride, and the fact that only 7.9% ± 1.6% and 3.9% ± 1.4% of the injected dose is still present in the blood at 50 and 90 min after injection, respectively. An additional calculation has been performed in which the contribution of the radioactivity uptake in the bone to the total absorbed dose by the bone (endosteum) is determined by entering the bone activity as the only source organ in the IDAC-Dose 2.1 radiation dosimetry software. A maximum of only 14% of the absorbed dose in the endosteum can be attributed to radiotracer accumulation in the bone. Although Figures 3 and 5 indicate that background activity in bone at 50 and 90 min is sufficiently low for identification of suggestive foci, high background noise might limit the interpretation of images acquired at 300 min after injection. Therefore, it can be estimated that the optimum time window extends from 50 to approximately 180 min after injection.

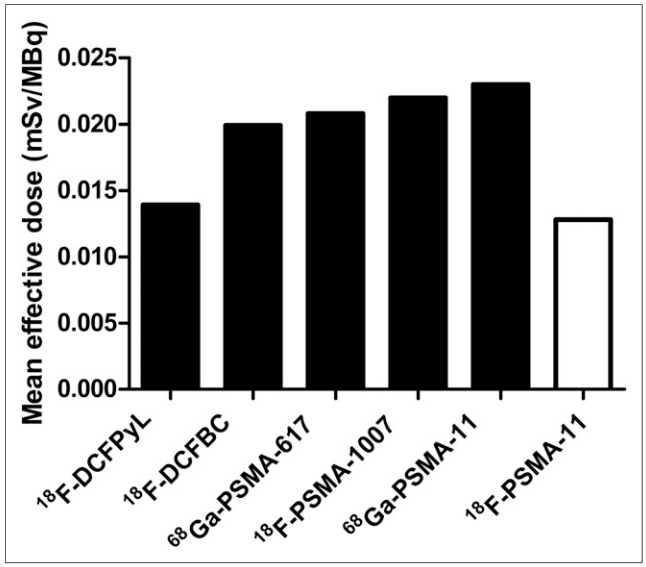

FIGURE 7. Comparison of mean effective doses of various recently developed PSMA PET radiotracers: ^{18}F-DCFPyL (*18*), ^{18}F-DCFBC (*32*), ^{68}Ga-PSMA-617 (*33*), ^{18}F-PSMA-1007 (*30*), ^{68}Ga-PSMA-11 (*29*), and ^{18}F-PSMA-11.

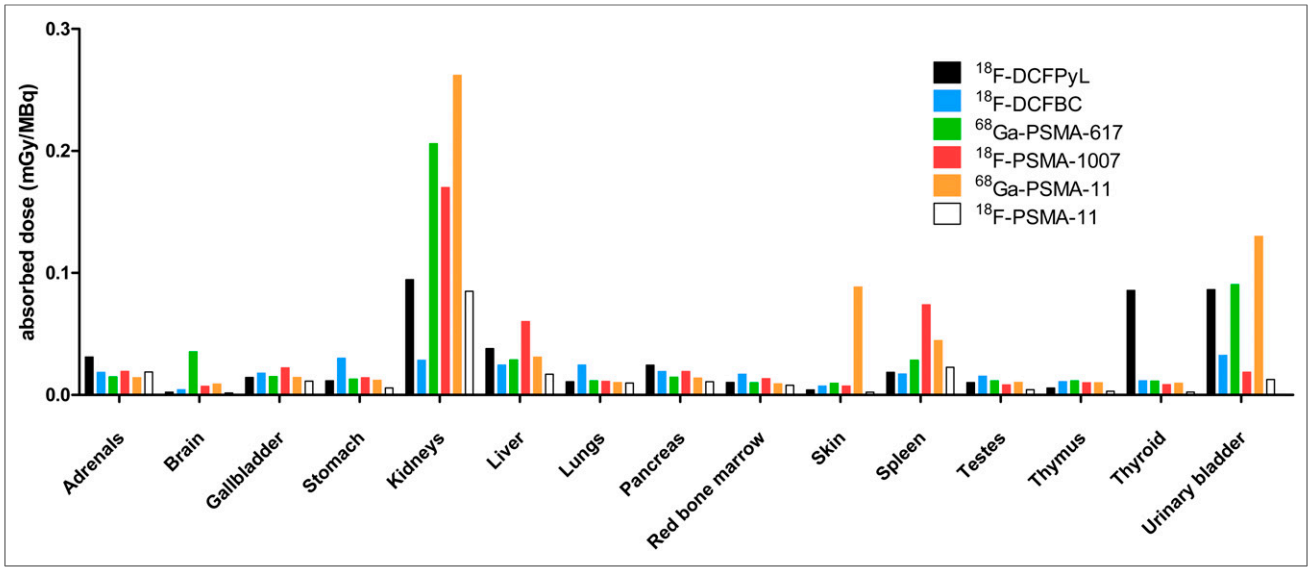

FIGURE 8. Comparison of absorbed dose per organ for various recently developed PSMA PET tracers: ^{18}F-DCFPyL (*18*), ^{18}F-DCFBC (*32*), ^{68}Ga-PSMA-617 (*33*), ^{18}F-PSMA-1007 (*30*), ^{68}Ga-PSMA-11 (*29*), and ^{18}F-PSMA-11.

However, defining the optimal time point for scanning will be a primary endpoint of the phase 2 trial.

The comparison of the defluorination rate and the absorbed bone dose between ^{18}F-PSMA-11 and other PSMA radiotracer analogs is complicated. On the one hand, not all studies applied a chromatographic technique (e.g., thin-layer chromatography) appropriate for the determination of the free ^{18}F-fluoride fraction in plasma. On the other hand, various radiation dosimetry software programs were used, such as IDAC-Dose 2.1 and OLINDA/EXM, which estimate an absorbed dose for the endosteum and the osteogenic cells, respectively. Replicating our ^{18}F-PSMA-11 dosimetry using OLINDA/EXM (Supplemental Table 1; supplemental materials are available at http://jnm.snmjournals.org) gives rise to an absorbed osteogenic cell dose of 0.0107 ± 0.0024 mGy/MBq, which is similar to ^{18}F-DCFPyl (0.00958 mGy/MBq) (*18*) and lower than other ^{18}F-labeled PSMA analogs, such as ^{18}F-PSMA-1007 (0.0155 mGy/MBq) (*30*) and ^{18}F-DCFBC (0.0182 mGy/MBq) (*32*). Nevertheless, comparison remains difficult because not every dosimetry study incorporated bone activity as a separate source organ.

The total effective dose of ^{18}F-PSMA-11(12.8 μSv/MBq) is similar to that of ^{18}F-DCFPyL (0.0139 mSv/MBq) (*18*) but lower than other known PSMA tracers, such as ^{18}F-DCFBC (0.0199 mSv/MBq) (*32*), ^{68}Ga-PSMA-617 (0.0208 mSv/MBq) (*33*), ^{18}F-PSMA-1007 (0.022 mSv/MBq) (*30*), and ^{68}Ga-PSMA-11 (0.023 mSv/MBq) (*29*) (Fig. 7). The low effective dose of ^{18}F-PSMA-11 is attributable to high urinary clearance, the low positron energy of ^{18}F, and the low absorbed doses for radiosensitive organs such as testes, thymus, and thyroid.

Figure 8 compares the most important corresponding organ-absorbed doses for the most commonly used PSMA PET tracers (^{18}F-DCFPyL (*18*), ^{18}F-DCFBC (*32*), ^{68}Ga-PSMA-617 (*33*), ^{18}F-PSMA-1007 (*30*), ^{68}Ga-PSMA-11 (*29*), and ^{18}F-PSMA-11). The most significant differences can be found in the absorbed dose of the kidneys, urinary bladder, liver, and spleen (Supplemental Table 2).

This paper compares effective radiation doses between different PSMA radiotracer analogs. Differences in the used scanners, scan protocols, and patient populations might also have an impact on the estimated radiation doses. Furthermore, the method for detection of metabolites focused only on the defluorination rate of ^{18}F-PSMA-11 and did not reinvestigate the stability of the PSMA-11 molecule in the human body, as Malik et al. (*20*) already demonstrated the stability of the PSMA-11 molecule over time in serum.

CONCLUSION

^{18}F-PSMA-11 shows rapid blood clearance and high renal excretion. The highest absorbed doses were in the kidneys (0.0850 ± 0.0164 mGy/MBq) and bladder (0.126 ± 0.00327 mGy/MBq). ^{18}F-PSMA-11 results in a mean effective dose of 12.8 ± 0.6 μSv/MBq and therefore has a radiation dose similar to ^{18}F-DCFPyL and lower than other PSMA PET agents. These results make ^{18}F-PSMA-11 a feasible PET tracer for subsequent patient studies determining scan protocols and diagnostic accuracy in prostate cancer.

DISCLOSURE

No potential conflict of interest relevant to this article was reported.

ACKNOWLEDGMENTS

We thank the cyclotron team and nursing staff of the Department of Nuclear Medicine of Ghent University Hospital for producing the radiotracer and for their outstanding cooperation.

KEY POINTS

QUESTION: This clinical study was conducted to assess the administration safety and biodistribution of ^{18}F-PSMA-11 in humans.

PERTINENT FINDINGS: The mean effective dose of ^{18}F-PSMA-11 was 12.8 ± 0.6 μSv/MBq. The highest absorbed doses were in the kidneys (0.0850 ± 0.0164 mGy/MBq) and bladder (0.126 ± 0.00327 mGy/MBq).

IMPLICATIONS FOR PATIENT CARE: With an effective dose lower than that of the most commonly used PET radiotracers, ^{18}F-PSMA-11 PET scans will reduce the exposure of patients to radiation.

REFERENCES

1. Zhou CK, Check DP, Lortet-Tieulent J, et al. Prostate cancer incidence in 43 populations worldwide: an analysis of time trends overall and by age group. *Int J Cancer.* 2016;138:1388–1400.
2. Paller CJ, Antonarakis ES. Management of biochemically recurrent prostate cancer after local therapy: evolving standards of care and new directions. *Clin Adv Hematol Oncol.* 2013;11:14–23.
3. McLeod DG. The effective management of biochemical recurrence in patients with prostate cancer. *Rev Urol.* 2005;7(suppl 5):S29–S36.
4. Kosuri S, Akhtar NH, Smith M, Osborne JR, Tagawa ST. Review of salvage therapy for biochemically recurrent prostate cancer: the role of imaging and rationale for systemic salvage targeted anti-prostate-specific membrane antigen radioimmunotherapy. *Adv Urol.* 2012;2012:921674.
5. Eiber M, Maurer T, Souvatzoglou M, et al. Evaluation of hybrid ^{68}Ga-PSMA ligand PET/CT in 248 patients with biochemical recurrence after radical prostatectomy. *J Nucl Med.* 2015;56:668–674.
6. PSA testing for the pretreatment staging and posttreatment management of prostate cancer. American Urological Association website. http://www.auanet.org/guidelines/prostate-specific-antigen-(2009-amended-2013). Published 2009. Amended 2013. Accessed July 10, 2019.
7. Buyyounouski MK, Hanlon AL, Eisenberg DF, et al. Defining biochemical failure after radiotherapy with and without androgen deprivation for prostate cancer. *Int J Radiat Oncol Biol Phys.* 2005;63:1455–1462.
8. Sweat SD, Pacelli A, Murphy GP, Bostwick DG. Prostate-specific membrane antigen expression is greatest in prostate adenocarcinoma and lymph node metastases. *Urology.* 1998;52:637–640.
9. Mannweiler S, Amersdorfer P, Trajanoski S, Terrett JA, King D, Mehes G. Heterogeneity of prostate-specific membrane antigen (PSMA) expression in prostate carcinoma with distant metastasis. *Pathol Oncol Res.* 2009;15:167–172.
10. Tian J-Y, Guo F-J, Zheng G-Y, Ahmad A. Prostate cancer: updates on current strategies for screening, diagnosis and clinical implications of treatment modalities. *Carcinogenesis.* 2018;39:307–317.
11. Roach PJ, Francis R, Emmett L, et al. The impact of ^{68}Ga-PSMA PET/CT on management intent in prostate cancer: results of an Australian prospective multicenter study. *J Nucl Med.* 2018;59:82–88.
12. Zacho HD, Nielsen JB, Afshar-Oromieh A, et al. Prospective comparison of ^{68}Ga-PSMA PET/CT, ^{18}F-sodium fluoride PET/CT and diffusion weighted-MRI at for the detection of bone metastases in biochemically recurrent prostate cancer. *Eur J Nucl Med Mol Imaging.* 2018; 45:1884–1897.
13. Mottet N, Bellmunt J, Bolla M, et al. EAU-ESTRO-SIOG guidelines on prostate cancer. Part 1: screening, diagnosis, and local treatment with curative intent. *Eur Urol.* 2017;71:618–629.
14. Kersemans K, De Man K, Courtyn J, et al. Automated radiosynthesis of Al [^{18}F]PSMA-11 for large scale routine use. *Appl Radiat Isot.* 2018;135:19–27.
15. Kesch C, Kratochwil C, Mier W, Kopka K, Giesel FL. ^{68}Ga or ^{18}F for prostate cancer imaging? *J Nucl Med.* 2017;58:687–688.
16. Sanchez-Crespo A. Comparison of gallium-68 and fluorine-18 imaging characteristics in positron emission tomography. *Appl Radiat Isot.* 2013;76:55–62.
17. Rowe SP, Gage KL, Faraj SF, et al. ^{18}F-DCFBC PET/CT for PSMA-based detection and characterization of primary prostate cancer. *J Nucl Med.* 2015;56:1003–1010.
18. Szabo Z, Mena E, Rowe SP, et al. Initial evaluation of [^{18}F]DCFPyL for prostate-specific membrane antigen (PSMA)-targeted PET imaging of prostate cancer. *Mol Imaging Biol.* 2015;17:565–574.
19. Cardinale J, Schäfer M, Benešová M, et al. Preclinical evaluation of ^{18}F-PSMA-1007, a new prostate-specific membrane antigen ligand for prostate cancer imaging. *J Nucl Med.* 2017;58:425–431.
20. Malik N, Baur B, Winter G, Reske SN, Beer AJ, Solbach C. Radiofluorination of PSMA-HBED via Al18F2+ chelation and biological evaluations in vitro. *Mol Imaging Biol.* 2015;17:777–785.
21. Boschi S, Lee JT, Beykan S, et al. Synthesis and preclinical evaluation of an Al 18 F radiofluorinated GLU-UREA-LYS (AHX)-HBED-CC PSMA ligand. *Eur J Nucl Med Mol Imaging.* 2016;43:2122–2130.
22. Giglio J, Zeni M, Savio E, Engler H. Synthesis of an Al^{18}F radiofluorinated GLU-UREA-LYS(AHX)-HBED-CC PSMA ligand in an automated synthesis platform. *EJNMMI Radiopharm Chem.* 2018;3:4.
23. Ahn S, Fessler JA. Globally convergent image reconstruction for emission tomography using relaxed ordered subsets algorithms. *IEEE Trans Med Imaging.* 2003;22:613–626.
24. Andersson M, Johansson L, Eckerman K, Mattsson S. IDAC-Dose 2.1, an internal dosimetry program for diagnostic nuclear medicine based on the ICRP adult reference voxel phantoms. *EJNMMI Res.* 2017;7:88.
25. ICRP publication 103: the 2007 recommendations of the International Commission on Radiological Protection. ICRP website. http://www.icrp.org/publication.asp?id=ICRP%20Publication%20103. Published 2007. Accessed July 10, 2019.
26. Jia ZS, Xie HX, Yang J, et al. Total blood volume of Asian patients undergoing cardiac surgery is far from that predicted by conventional methods. *J Cardiovasc Surg (Torino).* 2013;54:423–430.
27. Nair S, O'Brien SV, Hayden K, et al. Effect of a cooked meat meal on serum creatinine and estimated glomerular filtration rate in diabetes-related kidney disease. *Diabetes Care.* 2014;37:483–487.
28. Halma C. The serum creatinine level as a measure of renal function [in Dutch]. Dutch Journal of Medicine website. https://www.ntvg.nl/artikelen/het-serum-creatininegehalte-als-maat-voor-de-nierfunctie/volledig. Published August 5, 1990. Accessed July 10, 2019.
29. Afshar-Oromieh A, Hetzheim H, Kübler W, et al. Radiation dosimetry of ^{68}Ga-PSMA-11 (HBED-CC) and preliminary evaluation of optimal imaging timing. *Eur J Nucl Med Mol Imaging.* 2016;43:1611–1620.
30. Giesel FL, Hadaschik B, Cardinale J, et al. F-18 labelled PSMA-1007: biodistribution, radiation dosimetry and histopathological validation of tumor lesions in prostate cancer patients. *Eur J Nucl Med Mol Imaging.* 2017;44:678–688.
31. Pfob CH, Ziegler S, Graner FP, et al. Biodistribution and radiation dosimetry of ^{68}Ga-PSMA HBED CC—a PSMA specific probe for PET imaging of prostate cancer. *Eur J Nucl Med Mol Imaging.* 2016;43:1962–1970.
32. Cho SY, Gage KL, Mease RC, et al. Biodistribution, tumor detection, and radiation dosimetry of ^{18}F-DCFBC, a low-molecular-weight inhibitor of prostate-specific membrane antigen, in patients with metastatic prostate cancer. *J Nucl Med.* 2012;53:1883–1891.
33. Afshar-Oromieh A, Hetzheim H, Kratochwil C, et al. The theranostic PSMA ligand PSMA-617 in the diagnosis of prostate cancer by PET/CT: biodistribution in humans, radiation dosimetry, and first evaluation of tumor lesions. *J Nucl Med.* 2015;56:1697–1705.